

Inference after latent variable estimation for single-cell RNA sequencing data

Anna Neufeld [†], Lucy L. Gao [◦], Joshua Popp [△], Alexis Battle ^{△▽,‡}, and Daniela Witten ^{†‡}

[†] *Department of Statistics, University of Washington, Seattle, WA, USA*

[◦] *Department of Statistics and Actuarial Sciences, University of Waterloo, ON, Canada*

[△] *Department of Biomedical Engineering, Johns Hopkins University, Baltimore, MD, USA*

[▽] *Department of Computer Science, Johns Hopkins University, Baltimore, MD, USA*

[‡] *Department of Biostatistics, University of Washington, Seattle, WA, USA*

aneufeld@uw.edu

SUMMARY

In the analysis of single-cell RNA sequencing data, researchers often characterize the variation between cells by estimating a latent variable, such as cell type or pseudotime, representing some aspect of the individual cell’s state. They then test each gene for association with the estimated latent variable. If the same data are used for both of these steps, then standard methods for computing p-values and confidence intervals in the second step will fail to achieve statistical guarantees such as Type 1 error control. Furthermore, approaches such as sample splitting that can be applied to solve similar problems in other settings are not applicable in this context. In this paper, we introduce *count splitting*, a flexible framework that allows us to carry out valid inference in this setting, for virtually any latent variable estimation technique and inference approach, under a Poisson assumption. We demonstrate the Type 1 error control and power of count splitting in a simulation study, and apply count splitting to a dataset of pluripotent stem

cells differentiating to cardiomyocytes.

Key words: Poisson, binomial thinning, pseudotime, clustering, selective inference, sample splitting.

1. INTRODUCTION

Techniques for single-cell RNA sequencing (scRNA-seq) allow scientists to measure gene expression of huge numbers of individual cells in parallel. Researchers can then investigate how gene expression varies between cells of different states. In particular, we highlight two common questions that arise in the context of scRNA-seq data:

Question 1. *Which genes are differentially expressed along a continuous cellular trajectory?*

This trajectory might represent development, activity level of an important pathway, or *pseudotime*, a quantitative measure of biological progression through a process such as cell differentiation (Trapnell *and others*, 2014).

Question 2. *Which genes are differentially expressed between discrete cell types?*

These two questions are hard to answer because typically the cellular trajectory or the cell types are not directly observed, and must be estimated from the data. We can unify these two questions, and many others that arise in the analysis of scRNA-seq data, under a latent variable framework.

Suppose that we have mapped the scRNA-seq reads for n cells to p genes (or other functional units of interest). Then, the data matrix X has dimension $n \times p$, and X_{ij} is the number of reads from the i th cell that map to the j th gene. We assume that X is a realization of a random variable \mathbf{X} , and that the biological variation in $\mathbb{E}[\mathbf{X}]$ is explained by a set of latent variables $L \in \mathbb{R}^{n \times k}$. We wish to know which columns \mathbf{X}_j of \mathbf{X} are associated with L . As L is unobserved, the following two-step procedure seems natural:

Step 1: Latent variable estimation. Use X to compute $\hat{L}(X)$, an estimate of L .

Step 2: Differential expression analysis. For $j = 1, \dots, p$, test for association between \mathbf{X}_j and the columns of $\hat{L}(X)$.

While many authors have attempted to use this two-step procedure to answer Question 1 (see e.g. Cao *and others* 2019, Van den Berge *and others* 2020, and Qiu *and others* 2017) and Question 2 (see e.g. Aizarani *and others* 2019, Hwang *and others* 2018, and Satija *and others* 2015), the fact that $\hat{L}(X)$ is a function of the data means that Type 1 error control of standard statistical tests in Step 2 is compromised. Though no suitable solution has yet been proposed, the issues associated with this two-step process procedure are well-documented: Lähnemann *and others* (2020) cite the “double use of data” in differential expression analysis after clustering as one of the “grand challenges” in single cell RNA sequencing (Question 1), and Deconinck *and others* (2021) note that the “circularity” involved in the two-step process of trajectory analysis leads to “artificially low p-values” for differential expression (Question 2). We refer to the practice of using the same data X to select and test a null hypothesis as “double dipping”.

In this paper, we propose *count splitting*, a simple framework that allows us to carry out latent variable estimation and differential expression analysis without double dipping, so as to obtain p-values that control the Type 1 error for the null hypothesis that a given gene is not associated with an estimated latent variable.

In Section 2, we introduce the notation and models that will be used in this paper. In Section 3, we carefully examine existing methods for latent variable inference, and explain why they are not adequate in this setting. In Section 4 we introduce our proposed method, and in Sections 5 and 6 we demonstrate its merits on simulated and real data.

2. MODELS FOR SCRNA-SEQ DATA

Recall that X_{ij} is the number of reads mapping to the j th gene in the i th cell, and that $X \in \mathbb{R}^{n \times p}$ is a realization from \mathbf{X} . We assume that the entries in \mathbf{X} are independent, with

$$\mathbb{E}[\mathbf{X}_{ij}] = \gamma_i \Lambda_{ij}, \quad \log(\Lambda_{ij}) = \beta_{0j} + \beta_{1j}^T L_i, \quad i = 1, \dots, n, \quad j = 1, \dots, p, \quad (2.1)$$

where $\gamma_1, \dots, \gamma_n$ are cell-specific size factors that reflect technical variation in capture efficiency of the mRNA molecules between cells, the $n \times p$ matrix Λ represents biological variation, and the matrix $L \in \mathbb{R}^{n \times k}$ contains the unobserved latent variables. In (2.1), $\beta_{1j} \in \mathbb{R}^k$ and L_i is the i th row of L . Throughout this paper, we treat L , and thus Λ , as fixed. Estimating $\gamma_1, \dots, \gamma_n$ can be challenging. As size factor estimation is not the focus of this paper, we assume throughout that the γ_i are either known or have been accurately estimated (Vallejos *and others*, 2017).

Based on (2.1), in this paper we carry out the differential expression analysis step of the two-step process introduced in Section 1 by fitting a generalized linear model (GLM) with a log link function to predict X_j using $\widehat{L}(X)$, with the γ_i included as offsets. We note that while the notation introduced in the remainder of this section is specific to GLMs, the ideas in this paper can be extended to accommodate alternate methods for differential expression analysis, such as generalized additive models (as in Van den Berge *and others* 2020 and Trapnell *and others* 2014).

Under the assumption in (2.1), the columns of the matrix $\log(\Lambda)$ are linear combinations of the unobserved latent variables, which are the columns of L . However, they may not be linear combinations of the estimated latent variables, i.e. the columns of $\widehat{L}(X)$. Thus, we need to introduce additional notation to describe the population parameters that we target when we fit a GLM with $\widehat{L}(X)$, rather than L , as the predictor.

Let $p_\theta(\cdot)$ denote the density function of the distribution belonging to the exponential family specified by the GLM with mean θ . For any $Z \in \mathbb{R}^{n \times k}$ and random variable $\mathbf{X} \in \mathbb{R}^{n \times p}$, we define the population parameters targeted by fitting a GLM with a log link function to predict

X_j (drawn from \mathbf{X}_j) using Z , with the γ_i included as offsets, to be:

$$\left(\beta_0(Z, \mathbf{X}_j), \beta_1(Z, \mathbf{X}_j)\right) = \arg \max_{\alpha_0 \in \mathbb{R}, \alpha_1 \in \mathbb{R}^k} \left(\mathbb{E}_{\mathbf{X}_{1j}, \dots, \mathbf{X}_{nj}} \left[\sum_{i=1}^n \log \left(p_{\gamma_i \exp(\alpha_0 + \alpha_1^T Z_i)}(\mathbf{X}_{ij}) \right) \right] \right), \quad (2.2)$$

where the expectation in (2.2) is taken over the true joint distribution of $\mathbf{X}_{1j}, \dots, \mathbf{X}_{nj}$. We say that the j th gene is differentially expressed across a variable Z if $\beta_1(Z, \mathbf{X}_j) \neq 0$.

If the mean model in (2.1) holds and the true distribution of \mathbf{X}_{ij} belongs to the family specified by the GLM for $i = 1, \dots, n$, then $\beta_1(L, \mathbf{X}_j) = \beta_{1j}$ and $\beta_0(L, \mathbf{X}_j) = \beta_{0j}$ from (2.1). More generally, $\beta_0(Z, \mathbf{X}_j)$ and $\beta_1(Z, \mathbf{X}_j)$ in (2.2) are the parameters that make $\prod_{i=1}^n p_{\gamma_i \exp(\alpha_0 + \alpha_1^T Z_i)}(X_{ij})$ closest in Kullback-Leibler (KL) divergence to the true joint distribution for $\mathbf{X}_{1j}, \dots, \mathbf{X}_{nj}$ (see Section 2.4.3 of Wakefield 2013).

We denote the coefficient estimates that result from fitting a GLM with a log link function to predict a realized X_j using Z , with the γ_i included as offsets, as:

$$\left(\hat{\beta}_0(Z, X_j), \hat{\beta}_1(Z, X_j)\right) = \arg \max_{\alpha_0 \in \mathbb{R}, \alpha_1 \in \mathbb{R}^k} \sum_{i=1}^n \log \left(p_{\gamma_i \exp(\alpha_0 + \alpha_1^T Z_i)}(X_{ij}) \right). \quad (2.3)$$

For the majority of this paper, as in Wang *and others* (2018), we assume the model

$$\mathbf{X}_{ij} \stackrel{\text{ind.}}{\sim} \text{Poisson}(\gamma_i \Lambda_{ij}), \quad (2.4)$$

and let $p_\theta(\cdot)$ be a Poisson density. In Section 4.2, we discuss the case where \mathbf{X}_{ij} does not follow a Poisson distribution and/or $p_\theta(\cdot)$ is not a Poisson density.

3. EXISTING METHODS FOR LATENT VARIABLE INFERENCE

3.1 Motivating example

Throughout Section 3, we compare existing methods for differential expression analysis after latent variable estimation on a simple toy example. We generate 2,000 realizations of $\mathbf{X} \in \mathbb{R}^{200 \times 10}$, where $\mathbf{X}_{ij} \stackrel{\text{ind.}}{\sim} \text{Poisson}(\Lambda_{ij})$. For $i = 1, \dots, 200$, we let $\Lambda_{ij} = 1$ for $j = 1, \dots, 5$ and $\Lambda_{ij} = 10$ for $j = 6, \dots, 10$. (This is an example of the model defined in (2.1) and (2.4) with $\gamma_1 = \dots = \gamma_n = 1$

and $\beta_{1j} = 0$ for $j = 1, \dots, 10$.) Under this mechanism, each cell is drawn from the same distribution, and thus there is no true trajectory. Nevertheless, for each realized dataset X , we estimate a trajectory using the first principal component of the log-transformed data with a pseudocount of one. We then consider fitting Poisson GLMs to study differential expression. Since all columns of Λ are constant, $\beta_1(Z, \mathbf{X}_j) = 0$ for all j and for any $Z \in \mathbb{R}^n$ (see (2.2)). Therefore, any p-value quantifying the association between a gene and an estimated trajectory should follow a $\text{Unif}(0, 1)$ distribution. As we will see, most available approaches do not have this desired behavior.

3.2 Naive method

The *naive method* refers to using the same data for latent variable estimation and differential expression analysis, as in the two-step procedure in Section 1, without correcting for this double use. Variants of this method are used in the popular and highly-cited software packages **Seurat** (Satija *and others*, 2015) and **Monocle3** (Trapnell *and others*, 2014; Cao *and others*, 2020). The naive method attempts to do inference on the parameter $\beta_1(\hat{L}(X), \mathbf{X}_j)$, defined in (2.2), by regressing X_j on $\hat{L}(X)$. Using notation from Section 2, the resulting Wald p-values have the form

$$\Pr_{H_0: \beta_1(\hat{L}(X), \mathbf{X}_j)=0} \left(\left| \hat{\beta}_1(\hat{L}(X), \mathbf{X}_j) \right| \geq \left| \hat{\beta}_1(\hat{L}(X), X_j) \right| \right). \quad (3.5)$$

The right-hand side of the inequality in (3.5) uses the observed data to obtain both the predictor and the response, while the left-hand side does not. Thus, $\hat{\beta}_1(\hat{L}(X), X_j)$ is drawn from $\hat{\beta}_1(\hat{L}(\mathbf{X}), \mathbf{X}_j)$, not $\hat{\beta}_1(\hat{L}(X), \mathbf{X}_j)$. To state the issue in a different way, we used the data realization X to construct both the predictor $\hat{L}(X)$ and the response X_j in the GLM, and did not account for this double use in determining the distribution of the test statistic. Therefore, as shown in Figure 1, when we compute the p-value in (3.5) for many realizations of \mathbf{X} , the collection of p-values does not follow a $\text{Unif}(0, 1)$ distribution and fails to control the Type 1 error rate.

3.3 Cell splitting

In some settings, it is possible to overcome the issues associated with double dipping by splitting the observations into a training set and a test set, generating a hypothesis on the training set, and testing it on the test set (Cox, 1975). However, in the setting of this paper, splitting the cells in X does not allow us to bypass the issues of double dipping.

Why not? Suppose we estimate the latent variables using the cells in the training set, X^{train} . To test for differential expression using the cells in X^{test} , we need latent variable coordinates for the cells in X^{test} . However, it is not clear how to obtain latent variable coordinates for the cells in X^{test} that are only a function of the training set and not the test set (i.e. can be written as $\hat{L}(X^{\text{train}})$). In the simple example from Section 3.1, after computing the first principal axis of the log-transformed X^{train} matrix, we could consider projecting the log-transformed X^{test} onto this axis to obtain coordinates for the cells in X^{test} . Unfortunately, this projection step uses the data in X^{test} , and so the resulting estimated coordinates must be written as $\hat{L}(X^{\text{train}}, X^{\text{test}})$.

If we then fit a Poisson GLM to predict X_j^{test} using $\hat{L}(X^{\text{train}}, X^{\text{test}})$, the Wald p-values from this *cell splitting* procedure have the form

$$\Pr_{H_0: \beta_1(\hat{L}(X^{\text{train}}, X^{\text{test}}), \mathbf{X}_j^{\text{test}})=0} \left(\left| \hat{\beta}_1 \left(\hat{L}(X^{\text{train}}, X^{\text{test}}), \mathbf{X}_j^{\text{test}} \right) \right| \geq \left| \hat{\beta}_1 \left(\hat{L}(X^{\text{train}}, X^{\text{test}}), X_j^{\text{test}} \right) \right| \right). \quad (3.6)$$

Unfortunately, (3.6) suffers from the same issue as (3.5): the right-hand side of the inequality uses the same realization (X^{test}) to construct both the predictor and the response, whereas the left-hand side does not. Thus, the p-values from (3.6) do not follow a $\text{Unif}(0, 1)$ distribution, even when the columns of Λ are constants. Instead, they are anti-conservative, as shown in Figure 1.

3.4 Gene splitting

In the same spirit as cell splitting, we now consider *gene splitting*, which involves splitting the genes (features), rather than the observations, to form X^{train} and X^{test} . In this setting, $\hat{L}(X^{\text{train}})$ provides coordinates for all cells in X , and we can obtain p-values for each gene X_j that is not

in X^{train} by regressing X_j on $\widehat{L}(X^{\text{train}})$. The roles of X^{train} and X^{test} can be swapped to obtain p-values for the remaining genes. Gene splitting yields Wald p-values of the form

$$\begin{aligned} \Pr_{H_0: \beta_1(\widehat{L}(X^{\text{train}}), \mathbf{X}_j^{\text{test}})=0} \left(\left| \widehat{\beta}_1 \left(\widehat{L}(X^{\text{train}}), \mathbf{X}_j^{\text{test}} \right) \right| \geq \left| \widehat{\beta}_1 \left(\widehat{L}(X^{\text{train}}), X_j^{\text{test}} \right) \right| \right) & \quad \text{if } X_j \in X^{\text{test}}, \\ \Pr_{H_0: \beta_1(\widehat{L}(X^{\text{test}}), \mathbf{X}_j^{\text{train}})=0} \left(\left| \widehat{\beta}_1 \left(\widehat{L}(X^{\text{test}}), \mathbf{X}_j^{\text{train}} \right) \right| \geq \left| \widehat{\beta}_1 \left(\widehat{L}(X^{\text{test}}), X_j^{\text{train}} \right) \right| \right) & \quad \text{if } X_j \in X^{\text{train}}. \end{aligned}$$

As the coefficients on the right-hand side of these inequalities never use the same data to construct the predictor and the response, these p-values will be uniformly distributed over repeated realizations of \mathbf{X} when the columns of Λ are constants. However, they are fundamentally unsatisfactory in scRNA-seq applications where we wish to obtain a p-value for every gene *with respect to the same estimated latent variable*. Thus, gene splitting is not included in Figure 1.

3.5 Selective inference through conditioning

We next consider taking a *selective inference* approach (Fithian and others, 2014; Lee and others, 2016; Taylor and Tibshirani, 2015; Gao and others, 2020; Chen and Witten, 2022) to correct the p-values in (3.5). This involves fitting the same regression model as the naive method, but replacing (3.5) with the conditional probability

$$\Pr_{H_0: \beta_1(\widehat{L}(X), \mathbf{X}_j)=0} \left(\left| \widehat{\beta}_1 \left(\widehat{L}(X), \mathbf{X}_j \right) \right| \geq \left| \widehat{\beta}_1 \left(\widehat{L}(X), X_j \right) \right| \mid \widehat{L}(\mathbf{X}) = \widehat{L}(X) \right). \quad (3.7)$$

The inequality in (3.7) is identical to that in (3.5), but under the conditioning event, (3.7) can be rewritten as

$$\Pr_{H_0: \beta_1(\widehat{L}(X), \mathbf{X}_j)=0} \left(\left| \widehat{\beta}_1 \left(\widehat{L}(\mathbf{X}), \mathbf{X}_j \right) \right| \geq \left| \widehat{\beta}_1 \left(\widehat{L}(X), X_j \right) \right| \mid \widehat{L}(\mathbf{X}) = \widehat{L}(X) \right), \quad (3.8)$$

such that both the left-hand and right-hand sides of the inequality use the same data to construct the predictor and the response. Thus, over repeated realizations of \mathbf{X} when the columns of Λ are constants, the p-values in (3.7) follow a $\text{Unif}(0, 1)$ distribution.

We now argue that the approach in (3.7) is not suitable for the setting of this paper. First, the selective inference literature typically assumes normally distributed data to enable computation of

a modified version of (3.7). Because scRNA-seq data consists of non-negative integers, a normality assumption is not suitable. Second, as the conditioning event $\{\widehat{L}(\mathbf{X}) = \widehat{L}(X)\}$ in (3.7) must be explicitly characterized, each choice of $\widehat{L}(\cdot)$ will require its own bespoke strategy. This is problematic in the scRNA-seq setting, where many specialized techniques are used for data pre-processing, clustering, and trajectory estimation. Zhang *and others* (2019) overcome this challenge in the context of clustering by combining cell splitting (Section 3.3) with selective inference. The idea is to condition on the test set labeling event $\left\{\widehat{L}(X^{\text{train}}, \mathbf{X}^{\text{test}}) = \widehat{L}(X^{\text{train}}, X^{\text{test}})\right\}$, which can be easily characterized for any clustering algorithm provided that the estimated clusters are linearly separable. However, their work requires a normality assumption, and does not extend naturally to the setting of trajectory estimation.

Selective inference is omitted as a comparison method in Figure 1 because we are not aware of a way to compute (3.7) for Poisson data, even for our simple choice for $\widehat{L}(\cdot)$. In Appendix B of the supplementary materials, we show that the selective inference method of Gao *and others* (2020), which provides finite-sample valid inference after clustering for a related problem under a normality assumption, does not control the Type 1 error rate when applied to log-transformed Poisson data.

3.6 Jackstraw

Much of the difficulty with applying a selective inference approach in the setting of this paper lies in analytically characterizing the conditioning event in (3.7) and (3.8). An alternative approach is to try to compute a probability similar to (3.8), but without the conditioning event. While the distribution of $\widehat{\beta}_1(\widehat{L}(\mathbf{X}), \mathbf{X}_j)$ is typically not analytically tractable, its null distribution can be approximated via permutation. This is the idea behind the *jackstraw* method of Chung and Storey (2015), which was originally proposed to test for association between the principal components and features of a data matrix, and was later extended to the clustering setting (Chung, 2020).

To make our discussion of jackstraw congruent with the rest of this paper, we instantiate the framework to our latent variable GLM setting, and assume

$$\mathbf{X}_{ij} \stackrel{\text{ind.}}{\sim} H(\Lambda_{ij}), \quad \log(\Lambda_{ij}) = \beta_{0j} + \beta_{1j}L_i, \quad \beta_{1j}, L_i \in \mathbb{R}, \quad (3.9)$$

where $H(\mu)$ is a distribution parameterized by its mean μ . Compared to (2.1), we have omitted the size factors, have assumed that the latent variable is one-dimensional, and have assumed that each element of X is independently drawn from a distribution $H(\cdot)$.

To test if the j th gene is differentially expressed, jackstraw creates datasets $X^{\text{permute},b}$ for $b = 1, \dots, B$ by randomly permuting the j th column B times. Each dataset gives rise to a GLM coefficient $\hat{\beta}(\hat{L}(X^{\text{permute},b}), X_j^{\text{permute},b})$ and an associated standard error estimate $\widehat{\text{SE}}(\hat{\beta}(\hat{L}(X^{\text{permute},b}), X_j^{\text{permute},b}))$.

The p-value for the j th gene is computed as

$$\frac{1}{B} \sum_{b=1}^B \mathbf{1} \left\{ \frac{|\hat{\beta}_1(\hat{L}(X^{\text{permute},b}), X_j^{\text{permute},b})|}{\widehat{\text{SE}}(\hat{\beta}_1(\hat{L}(X^{\text{permute},b}), X_j^{\text{permute},b}))} \geq \frac{|\hat{\beta}_1(\hat{L}(X), X_j)|}{\widehat{\text{SE}}(\hat{\beta}_1(\hat{L}(X), X_j))} \right\}, \quad (3.10)$$

where $\mathbf{1}\{\cdot\}$ is an indicator function which evaluates to 1 if the inequality is true and 0 otherwise.

Under the null hypothesis that $\beta_{1j} = 0$ in (3.9), $X^{\text{permute},b}$ and X have the same distribution. Furthermore, both sides of the inequality in (3.10) use the same data realization to construct the predictor and the response. This suggests that under the null hypothesis that $\beta_{1j} = 0$ in (3.9), the distribution of the p-value in (3.10) will converge to $\text{Unif}(0, 1)$ as $B \rightarrow \infty$. This null hypothesis is slightly different than the ones tested in Sections 3.2–3.5, which involved association between the j th gene and an *estimated* latent variable.

Unfortunately, carrying out jackstraw as described above is computationally infeasible, as testing $H_0 : \beta_{1j} = 0$ for $j = 1, \dots, p$ requires $B \times p$ computations of $\hat{L}(\cdot)$. To improve computational efficiency, Chung and Storey (2015) suggest randomly choosing a set of s genes S_b to permute to obtain $X^{\text{permute},b}$ for $b = 1, \dots, B$. Then, the p-value for the j th gene is computed as

$$\frac{1}{B \times s} \sum_{b=1}^B \sum_{q \in S_b} \mathbf{1} \left\{ \frac{|\hat{\beta}_1(\hat{L}(X^{\text{permute},b}), X_q^{\text{permute},b})|}{\widehat{\text{SE}}(\hat{\beta}_1(\hat{L}(X^{\text{permute},b}), X_q^{\text{permute},b}))} \geq \frac{|\hat{\beta}_1(\hat{L}(X), X_j)|}{\widehat{\text{SE}}(\hat{\beta}_1(\hat{L}(X), X_j))} \right\}. \quad (3.11)$$

Since all p genes are compared to the same reference distribution, only B total computations of $\widehat{L}(\cdot)$ are needed. Unfortunately, the p-value in (3.11) only follows a $\text{Unif}(0, 1)$ distribution if the quantity on the right-hand side of the inequality in (3.11) follows the same distribution for all $j = 1, \dots, p$. This does not hold in the simple example from Section 3.1. In that example, the quantity on the right-hand side of the inequality in (3.11) has a different distribution for the genes with $\Lambda_{ij} = 1$ than those with $\Lambda_{ij} = 10$. While the collection of p-values aggregated across all of the genes appears to follow a $\text{Unif}(0, 1)$ distribution (Figure 1, left), the marginals are incorrect. That is, some genes have anti-conservative p-values (Figure 1, center) and others have overly conservative p-values (Figure 1, right).

3.7 PseudotimeDE

Song and Li (2021) recently proposed PseudotimeDE to test a gene's association with an estimated trajectory. Here, we present a slight modification of their proposal, which is tailored to our setting but does not change the fundamental properties with respect to the discussion. Implementation details are provided in Appendix C.

For $b = 1, \dots, B$, PseudotimeDE subsamples the cells in X to obtain X^b , computes $\widehat{L}(X^b)$, and then permutes this vector to create $\Pi(\widehat{L}(X^b))$, where $\Pi(\cdot)$ is a permutation operator. It then computes $\widehat{\beta}(\Pi(\widehat{L}(X^b)), X_j^b)$ for each of the B subsamples. The empirical p-value for the j th gene is given by

$$\frac{1}{B} \sum_{i=1}^B \mathbf{1} \left\{ \left| \widehat{\beta}(\Pi(\widehat{L}(X^b)), X_j^b) \right| \geq \left| \widehat{\beta}(\widehat{L}(X), X_j) \right| \right\}. \quad (3.12)$$

While it is not entirely clear what null hypothesis PseudotimeDE is designed to test, we can see that there is a problem with the p-value in (3.12). On the right-hand side of the inequality in (3.12), there is association between the predictor and the response in the GLM due to the fact that both are generated from the data X . On the left-hand side of the inequality in (3.12), permuting $\widehat{L}(X^b)$ disrupts the association between the predictor and the response. Thus, even in the absence

of any signal in the data, the quantity on the right-hand side of (3.12) does not have the same distribution as the quantity on the left-hand side of (3.12). As shown in Figure 1, under our simple example where there is no true trajectory, the p-values from (3.12) are anti-conservative.

4. COUNT SPLITTING

4.1 Method

In Sections 3.3 and 3.4, we saw that cell splitting and gene splitting are not suitable options for latent variable inference on scRNA-seq data. Here, we propose *count splitting*, which involves splitting the expression counts themselves, rather than the genes or the cells, to carry out latent variable estimation and differential expression analysis. The algorithm is as follows.

Algorithm 1 (Count splitting for latent variable inference) For a constant ϵ with $0 < \epsilon < 1$,

Step 0: Count splitting. Draw $\mathbf{X}_{ij}^{\text{train}} \mid \{\mathbf{X}_{ij} = X_{ij}\} \stackrel{\text{ind.}}{\sim} \text{Binomial}(X_{ij}, \epsilon)$, and let $X^{\text{test}} = X - X^{\text{train}}$.

Step 1: Latent variable estimation. Compute $\hat{L}(X^{\text{train}})$.

Step 2: Differential expression analysis. For $j = 1, \dots, p$,

- (a) Fit a GLM with a log link to predict X_j^{test} using $\hat{L}(X^{\text{train}})$, with the γ_i included as offsets. This provides $\hat{\beta}_1(\hat{L}(X^{\text{train}}), X_j^{\text{test}})$, an estimate of $\beta_1(\hat{L}(X^{\text{train}}), \mathbf{X}_j^{\text{test}})$.
- (b) Compute a Wald p-value for $H_0 : \beta_1(\hat{L}(X^{\text{train}}), \mathbf{X}_j^{\text{test}}) = 0$, which takes the form

$$Pr_{H_0: \beta_1(\hat{L}(X^{\text{train}}), \mathbf{X}_j^{\text{test}})=0} \left(\left| \hat{\beta}_1(\hat{L}(X^{\text{train}}), \mathbf{X}_j^{\text{test}}) \right| \geq \left| \hat{\beta}_1(\hat{L}(X^{\text{train}}), X_j^{\text{test}}) \right| \right). \quad (4.13)$$

Note that in Step 2(b), we are computing a standard GLM Wald p-value for a regression of X_j^{test} onto $\hat{L}(X^{\text{train}})$. The next result, which is a well-known property of the Poisson distribution (Durrett, 2019), guarantees that $\mathbf{X}^{\text{train}}$ and \mathbf{X}^{test} are independent.

Proposition 1 (Binomial thinning of Poisson processes) If $\mathbf{X}_{ij} \sim \text{Poisson}(\gamma_i \Lambda_{ij})$, then $\mathbf{X}_{ij}^{\text{train}}$ and $\mathbf{X}_{ij}^{\text{test}}$, as constructed in Algorithm 1, are independent. Furthermore, $\mathbf{X}_{ij}^{\text{train}} \sim \text{Poisson}(\epsilon \gamma_i \Lambda_{ij})$ and $\mathbf{X}_{ij}^{\text{test}} \sim \text{Poisson}((1 - \epsilon) \gamma_i \Lambda_{ij})$.

This means that in (4.13), under a Poisson model, the predictor and the response are independent on both sides of the inequality. Consequently, the p-value in (4.13) will retain all standard properties of a GLM Wald p-value: e.g. control of the Type 1 error rate for $H_0 : \beta_1 \left(\widehat{L}(X^{\text{train}}), \mathbf{X}_j^{\text{test}} \right) = 0$ when n is sufficiently large. Furthermore, when n is sufficiently large, we can invert the test in (4.13) to obtain confidence intervals with $100 \times (1 - \alpha)\%$ coverage for the parameter $\beta_1 \left(\widehat{L}(X^{\text{train}}), \mathbf{X}_j^{\text{test}} \right)$.

We now look more closely at the parameter $\beta_1 \left(\widehat{L}(X^{\text{train}}), \mathbf{X}_j^{\text{test}} \right)$. Suppose that for any matrix M and scalar a , the function $\widehat{L}(\cdot)$ satisfies $\widehat{L}(aM) \propto \widehat{L}(M)$. In this case, Proposition 1 says that $\widehat{L}(E[\mathbf{X}^{\text{train}}]) = \widehat{L}(\epsilon E[\mathbf{X}]) \propto \widehat{L}(E[\mathbf{X}])$. Furthermore, if $\log(E[\mathbf{X}_j]) = \beta_0 + \beta_1^T L_i$, then $\log(E[\mathbf{X}_j^{\text{test}}]) = \log(1 - \epsilon) + \beta_0 + \beta_1^T L_i$. Therefore, $\beta_1 \left(\widehat{L}(X^{\text{train}}), \mathbf{X}_j^{\text{test}} \right)$ is closely related to $\beta_1 \left(\widehat{L}(X), \mathbf{X}_j \right)$; the parameter (unsuccessfully) targeted by the naive method (Section 3.2).

REMARK 4.1 The key insight behind Algorithm 1 is that, under a Poisson assumption, a test for association between $\widehat{L}(X^{\text{train}})$ and $\mathbf{X}_j^{\text{test}}$ that uses $\widehat{L}(X^{\text{train}})$ and X_j^{test} will inherit standard statistical guarantees, despite the fact that $\widehat{L}(X^{\text{train}})$ and X_j^{test} are functions of the same data. This insight did not rely on the use of a GLM or a Wald test in Step 2 of Algorithm 1. Thus, other approaches could be used to quantify this association.

Figure 1 shows that count splitting with $\epsilon = 0.5$ produces uniformly distributed p-values for all genes in the example described in Section 3.1, using a Poisson GLM in Step 2 of Algorithm 1. We explore more values of ϵ and more complicated scenarios in Section 5.

Count splitting is a special case of “data fission”, proposed in a preprint by Leiner *and others* (2022) while this paper was in preparation. While the data fission framework is broad enough to

encompass this latent variable setting, Leiner *and others* (2022) focus on comparing data fission to sample splitting in supervised settings where the latter is an option. In unsupervised settings, where sample splitting is not an option (as seen in Section 3.3), ideas similar to count splitting have been applied by Batson *and others* (2019) and Chen *and others* (2021) for tasks such as evaluating the goodness-of-fit of a low-rank approximation of a matrix. We elaborate on connections to Batson *and others* (2019) in Appendix A of the supplementary materials. Finally, Gerard (2020) suggest applying binomial thinning to real scRNA-seq datasets to generate synthetic datasets to use for comparing and evaluating scRNA-seq software packages and methods, and this approach is used in the supplement of Sarkar and Stephens (2021) to compare various scRNA-seq models.

4.2 What if the data are not Poisson?

The independence between $\mathbf{X}_{ij}^{\text{train}}$ and $\mathbf{X}_{ij}^{\text{test}}$ in Proposition 1 holds if and only if \mathbf{X}_{ij} has a Poisson distribution (Kimeldorf *and others*, 1981). Thus, if we apply Algorithm 1 to data that are not Poisson, there will be dependence between the predictor and the response on the right-hand side of the inequality in (4.13), and the p-value in (4.13) will not be uniformly distributed under H_0 .

Wang *and others* (2018) argue that the Poisson model is sufficient to model scRNA-seq data. However, other models have been proposed. Townes *and others* (2019) advocate modeling the counts for each cell with a multinomial distribution. When the number of genes is large, the elements of the multinomial can be well-approximated by independent Poisson distributions, and indeed the authors rely on this approximation for computational reasons. Similarly, Batson *and others* (2019) assume that $\mathbf{X}_{ij} \sim \text{Binomial}(\Omega_{ij}, p_i)$, but note that typically Ω_{ij} is large and p_i is small, so that a Poisson approximation applies.

Sarkar and Stephens (2021) advocate pairing a Poisson *measurement* model for scRNA-seq data with a separate *expression* model to account for overdispersion compared to the Poisson

model. For example, a Gamma expression model leads to:

$$\mathbf{X}_{ij} \mid \{\tau_{ij} = \tau_{ij}\} \sim \text{Poisson}(\Lambda_{ij}\tau_{ij}), \quad \tau_{ij} \sim \text{Gamma}(b_j, b_j), \quad (4.14)$$

where we have omitted size factors for simplicity. This induces a negative binomial marginal distribution on \mathbf{X}_{ij} , where $E[\mathbf{X}_{ij}] = \Lambda_{ij}$ and $\text{Var}(\mathbf{X}_{ij}) = \Lambda_{ij} + \frac{\Lambda_{ij}^2}{b_j}$. If \mathbf{X}_{ij} is drawn from (4.14) and Algorithm 1 is applied, then $\mathbf{X}_{ij}^{\text{train}}$ and $\mathbf{X}_{ij}^{\text{test}}$ each follow negative binomial distributions, with $E[\mathbf{X}_{ij}^{\text{train}}] = \epsilon E[\mathbf{X}_{ij}]$ and $E[\mathbf{X}_{ij}^{\text{test}}] = (1 - \epsilon) E[\mathbf{X}_{ij}]$ (Harremoës *and others*, 2010). Our next result, proven in Appendix D.1, quantifies the correlation between $\mathbf{X}_{ij}^{\text{train}}$ and $\mathbf{X}_{ij}^{\text{test}}$ in this setting.

Proposition 2 Suppose that \mathbf{X}_{ij} follows a negative binomial distribution with expected value Λ_{ij} and variance $\Lambda_{ij} + \frac{\Lambda_{ij}^2}{b_j}$. If we perform Step 0 of Algorithm 1, then

$$\text{Cor}(\mathbf{X}_{ij}^{\text{train}}, \mathbf{X}_{ij}^{\text{test}}) = \frac{\sqrt{\epsilon(1 - \epsilon)}}{\sqrt{\epsilon(1 - \epsilon) + \frac{b_j^2}{\Lambda_{ij}^2} + \frac{b_j}{\Lambda_{ij}}}}. \quad (4.15)$$

To investigate the performance of count splitting under overdispersion, we generate datasets under (4.14) with $n = 200$ and $p = 10$. For each dataset, $\Lambda_{ij} = \Lambda = 5$ for $i = 1, \dots, n$ and $j = 1, \dots, p$, and $b_j = b$ for $j = 1, \dots, p$, so that every element of X is drawn from the same distribution. We generate 500 datasets for each value of $b \in \{50, 10, 5, 0.5\}$, so that $\frac{\Lambda}{b} \in \{0.1, 0.5, 1, 10\}$. Figure 2 displays the Wald p-values that result from running Algorithm 1 with a negative binomial GLM in Step 2, for all genes across all of the simulated datasets.

The denominator of (4.15) in Proposition 2 shows that $\frac{\Lambda}{b}$ determines the extent of correlation between $\mathbf{X}^{\text{train}}$ and \mathbf{X}^{test} in this setting. As shown in Figure 2, when $\frac{\Lambda}{b}$ is small, count splitting produces approximately uniformly distributed p-values, and thus comes very close to controlling the Type 1 error rate. As $\frac{\Lambda}{b}$ grows, the performance of count splitting approaches that of the naive method discussed in Section 3.2. Thus, count splitting tends to outperform the naive method, and in the case of extremely high overdispersion will be *no worse than* the naive method. For the real scRNA-seq dataset that we consider in Section 6, we show in Appendix E that the majority

of the estimated values of $\frac{\Lambda_{ij}}{b_j}$ are less than 1.

4.3 Choosing the tuning parameter ϵ

The parameter ϵ in Algorithm 1 governs a tradeoff between the information available for estimating L and the information available for carrying out inference. Proposition 3, proven in Appendix D.2, formalizes the intuition that X^{train} will look more similar to X when ϵ is large.

Proposition 3 If \mathbf{X}_{ij} follows a Poisson distribution and $\mathbf{X}_{ij}^{\text{train}} \sim \text{Binomial}(\mathbf{X}_{ij}, \epsilon)$, then

$$\text{Cor}(\mathbf{X}_{ij}, \mathbf{X}_{ij}^{\text{train}}) = \sqrt{\epsilon}. \quad (4.16)$$

Thus, as ϵ decreases, we expect $\widehat{L}(X^{\text{train}})$ and $\widehat{L}(X)$ to look less similar. This is a drawback, as scientists would ideally like to estimate L using *all* of the data. However, as ϵ increases, the power to reject false null hypotheses in Step 2(b) of Algorithm 1 decreases. Proposition 4, proven in Appendix D.3, quantifies this loss of power.

Proposition 4 Let $\mathbf{X}_{ij} \stackrel{\text{ind.}}{\sim} \text{Poisson}(\gamma_i \exp(\beta_{0j} + \beta_{1j} L_i))$. Then

$$\text{Var}\left(\widehat{\beta}_1(L, \mathbf{X}_j^{\text{test}})\right) \approx \frac{1}{1-\epsilon} \text{Var}\left(\widehat{\beta}_1(L, \mathbf{X}_j)\right).$$

In the ideal setting where $\widehat{L}(X^{\text{train}}) = L$ (and where $L \in \mathbb{R}^{n \times 1}$ for simplicity), using $\mathbf{X}_j^{\text{test}}$ rather than \mathbf{X}_j as the response inflates the variance of the estimated slope coefficient by a factor of $\frac{1}{1-\epsilon}$. Thus, when ϵ is large, Step 2(b) of Algorithm 1 has lower power.

5. SIMULATION STUDY

5.1 Data generating mechanism

We generate data from (2.1) and (2.4) with $n = 200$ and $p = 100$. We generate the size factors $\gamma_i \stackrel{\text{ind.}}{\sim} \text{Gamma}(10, 10)$ and treat them as known. Throughout this section, whenever we perform

count splitting, we fit a Poisson GLM in Step 2 of Algorithm 1 and report Wald p-values.

In this section, we investigate the performance of count splitting under two data-generating mechanisms: one generates a true continuous trajectory and the other generates true clusters. To generate data with an underlying trajectory, we set $L = (I_n - \frac{1}{n}11^T) Z$, where $Z_i \stackrel{\text{ind.}}{\sim} N(0, 1)$. Under (2.1), L is the first principal component of the matrix $\log(\Lambda)$. To estimate L , we take the first principal component of the matrix $\log(\text{diag}(\gamma)^{-1}X + 11^T)$. To generate data with underlying cell types, we let $L_i \stackrel{\text{ind.}}{\sim} \text{Bernoulli}(0.5)$ in (2.1), indicating membership in one of two cell types. We estimate L by running k -means with $k = 2$ on the matrix $\log(\text{diag}(\gamma)^{-1}X + 11^T)$. (In each case, we have used a pseudocount of one to avoid taking the log of zero.)

In our primary simulation setting, the value β_{0j} for each gene is randomly chosen to be either $\log(3)$ or $\log(25)$ with equal probability, such that the data includes a mix of low-intercept and high-intercept genes. For each dataset, we let $\beta_{1j} = 0$ for 90% of the p genes. Under (2.1), $\Lambda_{1j} = \dots = \Lambda_{nj}$ for these genes and thus $\beta_1(Z, \mathbf{X}_j) = 0$ for any estimated latent variable Z . Thus, we refer to these as the null genes. The remaining 10% of the genes have the same non-zero value of β_{1j} ; these are the differentially-expressed genes. For each latent variable setting, we generate 1,000 datasets for each of 15 equally-spaced values of β_{1j} in $[0.18, 3]$.

5.2 Type 1 error results

Figure 3 shows that count splitting controls the Type 1 error rate for a range of ϵ values for the 90% of genes for which $\beta_{1j} = 0$ in datasets that are generated as specified in Section 5.1.

5.3 Quality of estimate of L

As mentioned in Section 4.3, smaller values of ϵ in count splitting compromise our ability to accurately estimate the unobserved latent variable L . To quantify the quality of our estimate of L , in the trajectory estimation case we compute the absolute value of the correlation between L

and $\widehat{L}(X^{\text{train}})$, and in the clustering setting we compute the adjusted Rand index (Hubert and Arabie, 1985) between L and $\widehat{L}(X^{\text{train}})$. The results are shown in Figure 4. Here, we consider three settings for the value of β_{0j} : (i) each gene is equally likely to have $\beta_{0j} = \log(3)$ or $\beta_{0j} = \log(25)$ (as in Section 5.2); (ii) all genes have $\beta_{0j} = \log(3)$ (“100% low-intercept” setting); and (iii) all genes have $\beta_{0j} = \log(25)$ (“100% high-intercept” setting). The 100% low-intercept setting represents a case where the sequencing was less deep, and thus the data more sparse.

After taking a log transformation, the genes with $\beta_{0j} = \log(3)$ have higher variance than those with $\beta_{0j} = \log(25)$. Thus, there is more noise in the “100% low-intercept” setting than in the “100% high-intercept” setting. As a result, for a given value of ϵ , the “100% low-intercept” setting results in the lowest-quality estimate of L . Estimation of L is particularly poor in the “100% low-intercept” setting when ϵ is small, since then X^{train} contains many zero counts. This suggests that count splitting, especially with small values of ϵ , is less effective on shallow sequencing data.

5.4 Power results

For each dataset and each gene, we compute the true parameter $\beta_1(\widehat{L}(X^{\text{train}}), \mathbf{X}_j^{\text{test}})$ defined in (2.2). For a Poisson GLM (i.e. $p_\theta(\cdot)$ in (2.2) is the density of a $\text{Poisson}(\theta)$ distribution), it is straightforward to show that we can compute $\beta_1(\widehat{L}(X^{\text{train}}), \mathbf{X}_j^{\text{test}})$ by fitting a Poisson GLM with a log link to predict $E[\mathbf{X}_j]$ using $\widehat{L}(X^{\text{train}})$, with the γ_i included as offsets.

Figure 5 shows that our ability to reject the null hypothesis depends on this true parameter, as well as on the value of ϵ . These results are shown in the setting where 50% of the genes have intercept $\log(3)$ and the other 50% have intercept $\log(25)$. The impact of ϵ on power is more apparent for genes with smaller intercepts, as these genes have even less information left over for inference when $(1 - \epsilon)$ is small. This result again suggests that count splitting will work best on deeply sequenced data where expression counts are less sparse.

As suggested by Section 4.3, Figures 4 and 5 show a tradeoff in choosing ϵ : a larger value of

ϵ improves latent variable estimation, but yields lower power for differential expression analysis.

5.5 Coverage results

For each dataset and each gene, we compute a 95% Wald confidence interval for the slope parameter in the GLM. We then check if the confidence interval contains the target parameter $\beta_1 \left(\widehat{L}(X^{\text{train}}), \mathbf{X}_j^{\text{test}} \right)$, defined in (2.2) and computed as in Section 5.4. As shown in Table 1, these intervals achieve nominal coverage.

6. APPLICATION TO CARDIOMYOCYTE DIFFERENTIATION DATA

Elorbany *and others* (2022) collect single-cell RNA-sequencing data over seven unique time points in 19 human cell lines. The cells are known to be differentiating from induced pluripotent stem cells to cardiomyocytes. In this section, we analyze a subsample of 10,000 cells from one single lineage of this differentiating trajectory. We ignore the true temporal information (the known day of collection) and estimate a continuous differentiation trajectory. We then study differential expression of genes across this trajectory.

To estimate continuous differentiation trajectories, we use a function $\widehat{L}(\cdot)$ that includes several preprocessing steps, followed by the `orderCells()` function from the `Monocle3` package in R (Cao *and others*, 2019). Details are given in Appendix F. We conduct all preprocessing steps within the function $\widehat{L}(\cdot)$, and thus downstream of count splitting, because count splitting can only be applied to integer-valued data and because we wish to avoid introducing dependence between the training set and the test set via shared preprocessing. To estimate the size factors $\gamma_1, \dots, \gamma_n$ in (2.4), we let $\hat{\gamma}_i(X)$ be the normalized row sums of the expression matrix X , as is the default in the `Monocle3` package. We perform count splitting with $\epsilon = 0.5$.

Throughout this section, for $j = 1, \dots, p$, we compare three methods:

Full naive: Fit a Poisson GLM of X_j on $\widehat{L}(X)$ with $\hat{\gamma}_i(X)$ included as offsets.

Count splitting: Fit a Poisson GLM of X_j^{test} on $\widehat{L}(X^{\text{train}})$ with $\hat{\gamma}_i(X^{\text{train}})$ included as offsets.

Test naive: Fit a Poisson GLM of X_j^{test} on $\widehat{L}(X^{\text{test}})$ with $\hat{\gamma}_i(X^{\text{test}})$ included as offsets.

For each method, we report the Wald p-values for the slope coefficients. The test naive method is included to facilitate understanding of the results from the other two methods. We show in Appendix E that the estimated overdispersion parameters are relatively small for this dataset, justifying the use of count splitting and Poisson GLMs in each of the methods above.

We first analyze all 10,000 cells. There is a true differentiation trajectory in this dataset: cells were sampled at seven different time points from a directed differentiation protocol, displaying the expected progression of marker gene expression over time as well as observable phenotypic changes (Elorban *and others*, 2022). We focus on a subset of $p = 2,500$ high-variance genes that were selected from the original 21,971 genes in the data (see Appendix F for details). The left panel of Figure 6 displays the count splitting p-values for differential expression of these 2,500 genes against the naive method p-values.

We first note the general agreement between the three methods: genes that have small p-values with one method generally have small p-values with all the methods. Thus, count splitting tends to identify the same differentially expressed genes as the naive methods when there is a true trajectory in the data. That said, we do notice that the full naive method tends to give smaller p-values than count splitting. There are two possible reasons for this: (i) the p-values from the naive method may be artificially small due to the fact that it double dips in the data, or (ii) it might be due to the fact that the full naive method uses twice as much data. In this setting, it seems that (ii) is the correct explanation: the test naive method (which double dips but uses the same amount of data as count splitting both to estimate L and to test the null hypothesis) yields comparably sized p-values to count splitting. It seems that there is enough true signal in this data that most of the genes identified by the naive methods as differentially expressed are truly differentially expressed, rather than false positives attributable to double dipping.

Next, we subset the 10,000 cells to only include the 2,209 cells that were measured at the first time point (day 0) of the experiment, before differentiation had begun. Despite knowing that the cells should be homogeneous and not contain a meaningful trajectory, we apply $\widehat{L}(\cdot)$ to estimate pseudotime. We suspect that in this setting, any association seen between pseudotime and the genes is due to overfitting or random noise. We select a new set of 2,500 high variance genes using this subset of cells. The right panel of Figure 6 shows uniform QQ plots of the p-values for these 2,500 genes from each of the three methods. In the absence of real differentiation signal, the p-values should follow a uniform distribution. We see that count splitting controls the Type 1 error rate, while the naive methods do not.

In summary, count splitting detects differentially expressed genes when there is true signal in the data, and protects against Type 1 errors when there is no true signal in the data.

7. DISCUSSION

Under a Poisson assumption, count splitting provides a flexible framework for carrying out valid inference after latent variable estimation that can be applied to virtually any latent variable estimation method and inference technique. This has important applications in the growing field of pseudotime or trajectory analysis, as well as in cell type analysis.

We expect count splitting to be useful in situations other than those considered in this paper. For example, as explored in Appendix B, count splitting can be used to test the overall difference in means between two estimated clusters, as considered by Gao *and others* (2020) and Chen and Witten (2022). As suggested in related work by Batson *and others* (2019), Chen *and others* (2021), and Gerard (2020), count splitting could be used for model selection tasks such as choosing how many dimensions to keep when reducing the dimension of Poisson scRNA-seq data. Finally, count splitting may lead to power improvements over sample splitting for Poisson data on tasks where the latter is an option (Leiner *and others*, 2022).

In this paper, we assume that after accounting for biological variation due to size factors and after allowing for heterogenous expected expression across cells and genes, the scRNA-seq data follows a Poisson distribution. Some authors have argued that even after accounting for these factors, scRNA-seq data is overdispersed relative to the Poisson. As discussed in Section 4.2, count splitting fails to provide independent training and testing sets when applied to negative binomial data. Leiner *and others* (2022) suggest that inference can be carried out in this setting by working with the conditional distribution of $X^{\text{test}} \mid X^{\text{train}}$, which they derive for negative binomial data under count splitting. Unfortunately, this conditional distribution does not lend itself to inference on parameters of interest. In future work, we will consider splitting algorithms for overdispersed count distributions.

Code for reproducing the simulations and real data analysis in this paper is available at github.com/anna-neufeld/countsplitted-paper. An R package with tutorials is available at anna-neufeld.github.io/countsplitted.

8. ACKNOWLEDGEMENTS

Anna Neufeld and Daniela Witten were funded by the Simons Foundation (Simons Investigator Award in Mathematical Modeling of Living Systems). Lucy Gao was supported by the Natural Sciences and Engineering Research Council of Canada (Discovery Grants). Alexis Battle was funded by NIGMS MIRA - 1R35GM139580.

REFERENCES

- AIZARANI, N. *and others*. (2019). A human liver cell atlas reveals heterogeneity and epithelial progenitors. *Nature* **572**(7768), 199–204.
- BATSON, J., ROYER, L. AND WEBBER, J. (2019). Molecular cross-validation for single-cell RNA-seq. *BioRxiv*, 786269.

- CAO, J. *and others.* (2019). The single-cell transcriptional landscape of mammalian organogenesis. *Nature* **566**, 496—502.
- CAO, J *and others.* (2020). A human cell atlas of fetal gene expression. *Science* **370**(6518), eaba7721.
- CHEN, F., ROCH, S., ROHE, K. AND YU, S. (2021). Estimating graph dimension with cross-validated eigenvalues. *arXiv:2108.03336*.
- CHEN, Y. T. AND WITTEN, D. M. (2022). Selective inference for k-means clustering. *arXiv:2203.15267*.
- CHUNG, N. C. (2020). Statistical significance of cluster membership for unsupervised evaluation of cell identities. *Bioinformatics* **36**(10), 3107–3114.
- CHUNG, N. C. AND STOREY, J. D. (2015). Statistical significance of variables driving systematic variation in high-dimensional data. *Bioinformatics* **31**(4), 545–554.
- CHUNG, N. C., STOREY, J. D. AND HAO, W. (2021). *Jackstraw: statistical inference for unsupervised learning*. R package version 1.3.1.
- COX, D. R. (1975). A note on data-splitting for the evaluation of significance levels. *Biometrika* **62**(2), 441–444.
- DECONINCK, L. *and others.* (2021). Recent advances in trajectory inference from single-cell omics data. *Current Opinion in Systems Biology* **27**, 100344.
- DURRETT, R. (2019). *Probability: theory and examples*, Volume 49. Cambridge University Press.
- ELORBANY, R. *and others.* (2022). Single-cell sequencing reveals lineage-specific dynamic genetic regulation of gene expression during human cardiomyocyte differentiation. *PLoS Genetics* **18**(1), e1009666.

- FITHIAN, W., SUN, D. AND TAYLOR, J. (2014). Optimal inference after model selection. *arXiv:1410.2597*.
- GAO, L. L., BIEN, J. AND WITTEN, D. (2020). Selective inference for hierarchical clustering. *arXiv:2012.02936*.
- GERARD, D. (2020). Data-based RNA-seq simulations by binomial thinning. *BMC Bioinformatics* **21**(1), 1–14.
- HAGHVERDI, L. *and others*. (2018). Batch effects in single-cell RNA-sequencing data are corrected by matching mutual nearest neighbors. *Nature Biotechnology* **36**(5), 421–427.
- HARREMOËS, P., JOHNSON, O. AND KONTOYIANNIS, I. (2010). Thinning, entropy, and the law of thin numbers. *IEEE Transactions on Information Theory* **56**(9), 4228–4244.
- HUBERT, L. AND ARABIE, P. (1985). Comparing partitions. *Journal of Classification* **2**(1), 193–218.
- HWANG, B., LEE, J. H. AND BANG, D. (2018). Single-cell RNA sequencing technologies and bioinformatics pipelines. *Experimental & Molecular Medicine* **50**(8), 1–14.
- KIMELDORF, G., PLACHKY, D. AND SAMPSON, A. R. (1981). A simultaneous characterization of the Poisson and Bernoulli distributions. *Journal of Applied Probability* **18**(1), 316–320.
- LÄHNEMANN, D. *and others*. (2020). Eleven grand challenges in single-cell data science. *Genome Biology* **21**(1), 1–35.
- LEE, J. D., SUN, D. L., SUN, Y. AND TAYLOR, J. E. (2016). Exact post-selection inference, with application to the lasso. *The Annals of Statistics* **44**(3), 907–927.
- LEINER, J., DUAN, B., WASSERMAN, L. AND RAMDAS, A. (2022). Data fission: splitting a single data point. *arXiv:2112.11079v4*.

- LUN, AARON T. L., MCCARTHY, DAVIS J. AND MARIONI, JOHN C. (2016). A step-by-step workflow for low-level analysis of single-cell RNA-seq data with Bioconductor. *F1000Res.* **5**, 2122.
- PLINER, H., QIU, X., TRAPNELL, C. AND EWING, B. (2020). *Monocle3*. R package version 1.2.9. <https://cole-trapnell-lab.github.io/monocle3/>.
- QIU, X. *and others*. (2017). Single-cell mRNA quantification and differential analysis with Census. *Nature Methods* **14**(3), 309–315.
- SARKAR, A. AND STEPHENS, M. (2021). Separating measurement and expression models clarifies confusion in single-cell RNA sequencing analysis. *Nature Genetics* **53**(6), 770–777.
- SATIJA, R. *and others*. (2015). Spatial reconstruction of single-cell gene expression data. *Nature Biotechnology* **33**, 495–502.
- SONG, D. AND LI, J. J. (2021). PseudotimeDE: inference of differential gene expression along cell pseudotime with well-calibrated p-values from single-cell RNA sequencing data. *Genome Biology* **22**(1), 1–25.
- SONG, D., LIU, T. AND NGUYEN, H. (2021). *PseudotimeDE*. R package version 1.0.0.
- TAYLOR, J. AND TIBSHIRANI, R. J. (2015). Statistical learning and selective inference. *Proceedings of the National Academy of Sciences* **112**(25), 7629–7634.
- TOWNES, F. W., HICKS, S. C., ARYEE, M. J. AND IRIZARRY, R. A. (2019). Feature selection and dimension reduction for single-cell RNA-Seq based on a multinomial model. *Genome Biology* **20**(1), 1–16.
- TRAPNELL, C *and others*. (2014). The dynamics and regulators of cell fate decisions are revealed by pseudotemporal ordering of single cells. *Nature Biotechnology* **32**(4), 381–386.

- VALLEJOS, C. A. *and others.* (2017). Normalizing single-cell RNA sequencing data: challenges and opportunities. *Nature Methods* **14**(6), 565–571.
- VAN DEN BERGE, K. *and others.* (2020). Trajectory-based differential expression analysis for single-cell sequencing data. *Nature Communications* **11**(1), 1–13.
- WAKEFIELD, J. (2013). *Bayesian and frequentist regression methods*, Volume 23. Springer.
- WANG, J. *and others.* (2018). Gene expression distribution deconvolution in single-cell RNA sequencing. *Proceedings of the National Academy of Sciences* **115**(28), E6437–E6446.
- ZHANG, J. M., KAMATH, G. M. AND DAVID, N. T. (2019). Valid post-clustering differential analysis for single-cell RNA-Seq. *Cell Systems* **9**(4), 383–392.
- ZHENG, S. C. *and others.* (2022). Universal prediction of cell cycle position using transfer learning. *Genome Biology* **23**, 41.

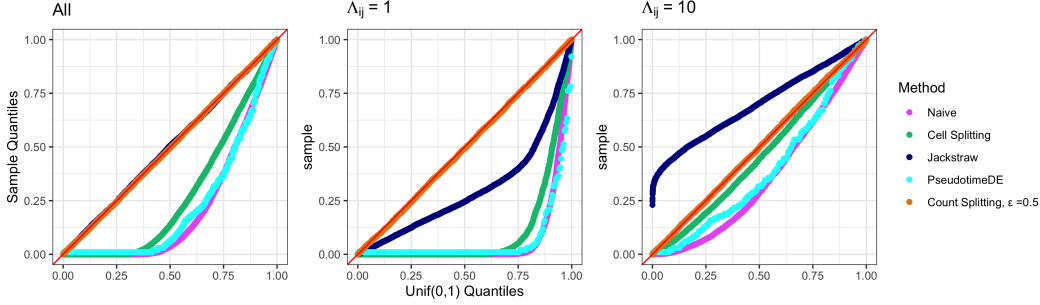


Fig. 1. Uniform QQ-plots of p-values for the $p = 10$ genes in each of 2000 datasets generated as described in Section 3.1. The left-hand panel shows all of the genes aggregated, whereas the center and right panels break the results down by the value of Λ_{ij} .

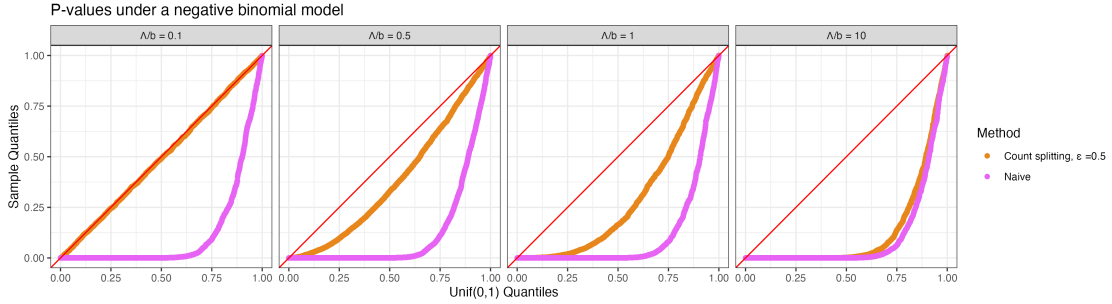


Fig. 2. Uniform QQ-plots for p-values across all genes and all realizations of \mathbf{X} for the simulation described in Section 4.2. Results are broken down by the magnitude of $\frac{\Lambda}{b}$. As $\frac{\Lambda}{b}$ increases, the correlation between $\mathbf{X}^{\text{train}}$ and \mathbf{X}^{test} increases, and the performance of count splitting approaches that of the naive method.

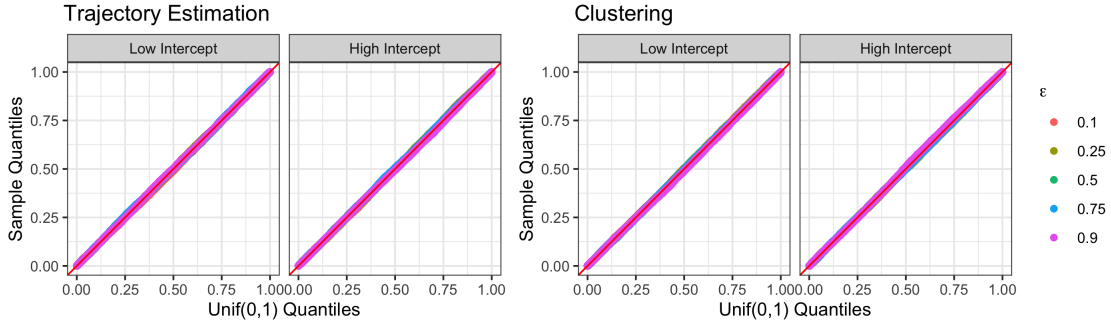


Fig. 3. Uniform QQ plots of GLM p-values for all null genes from the simulations described in Section 5.1. Plots are broken down into low-intercept and high-intercept genes. Results for five values of ϵ are displayed.

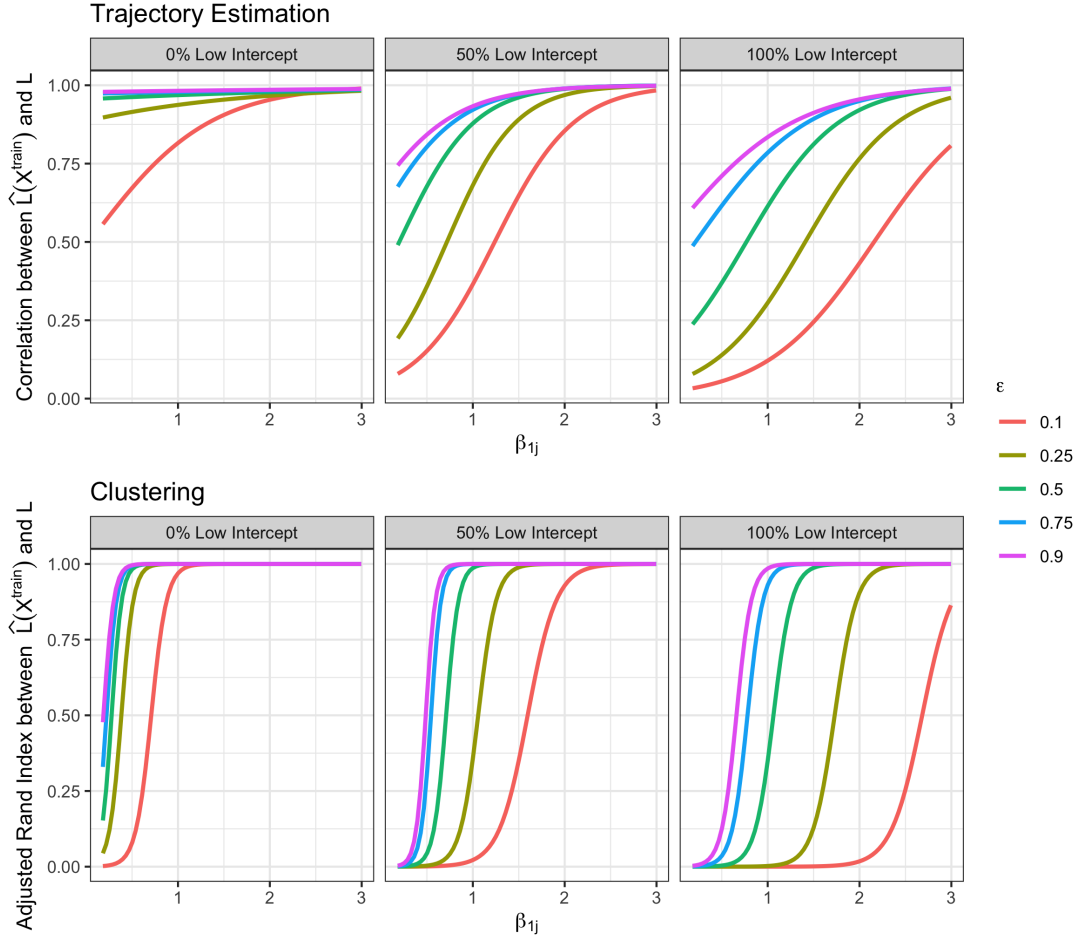


Fig. 4. Quality of estimate of L , as defined in Section 5.3, as a function of β_{1j} and the percent of low-intercept genes in the dataset. Results are averaged over 1000 data realizations for each combination of parameters.

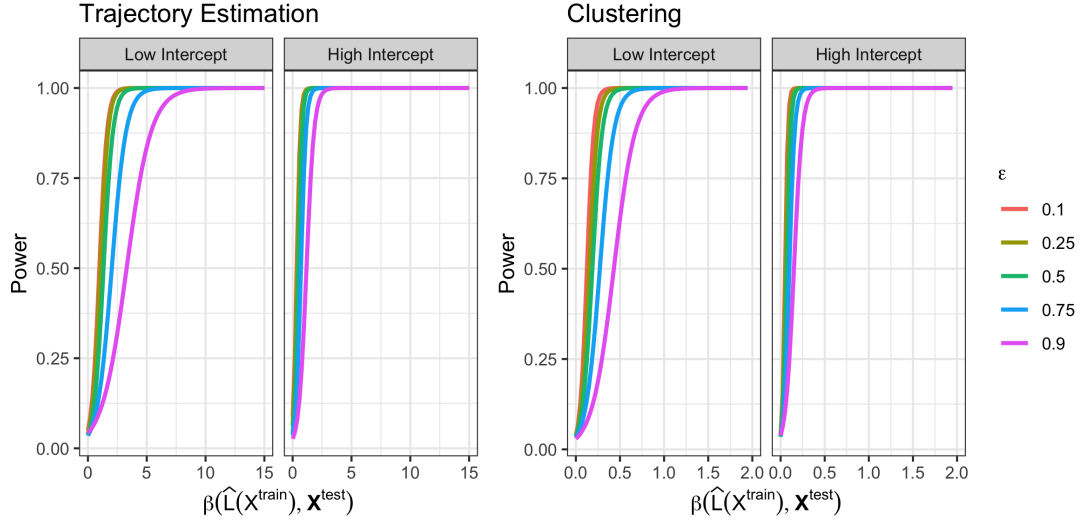


Fig. 5. The proportion of null hypotheses that are rejected, aggregated across all non-null genes for all datasets generated with 50% low-intercept and 50% high-intercept genes. The parameter $\beta_1 \left(\hat{L}(X^{\text{train}}), \mathbf{X}_j^{\text{test}} \right)$ is defined in (2.2).

	Trajectory Estimation		Clustering	
	Low Intercept	High Intercept	Low Intercept	High Intercept
Null genes	0.950	0.950	0.950	0.950
Non-null genes	0.955	0.955	0.955	0.955

Table 1. The proportion of 95% confidence intervals that contain $\beta_1 \left(\hat{L}(X^{\text{train}}), \mathbf{X}_j^{\text{test}} \right)$, aggregated across genes and across values of ϵ .

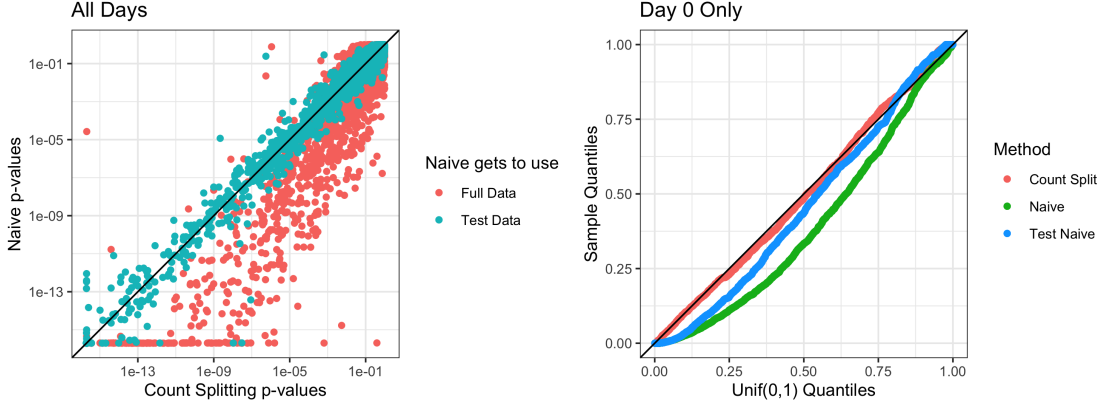


Fig. 6. *Left*: Count splitting p-values vs. naive p-values for 2,500 genes, on a log scale, when all 10,000 cells are used in the analysis. *Right*: Uniform QQ plot of p-values for 2,500 genes obtained from each method when only the Day 0 cells are used.

APPENDIX

A. CONNECTIONS TO BATSON *and others* (2019)

To evaluate the goodness-of-fit of low-rank approximations of scRNA-seq expression matrices, with the ultimate goal of selecting optimal hyperparameters (such as the number of principal components to keep), Batson *and others* (2019) seek to obtain independent training and test sets. They propose *molecular cross validation* (MCV), a method for obtaining such sets under the assumption that $X_{ij} \sim \text{Binomial}(\Omega_{ij}, p_i)$, where Ω_{ij} is the true number of mRNA molecules for gene j in cell i and p_i is the probability that a molecule in cell i is observed. The splitting method involves three steps:

1. $X_{ij}^{\text{train}} \sim \text{Binomial}(X_{ij}, \epsilon)$
2. $X_{ij}^{\text{both}} \sim \text{Binomial}(X_{ij}^{\text{train}}, p_i'')$
3. $X_{ij}^{\text{test}} = X_{ij} - X_{ij}^{\text{train}} + X_{ij}^{\text{both}}$.

Under the binomial assumption, if p_i'' is chosen appropriately, then X_{ij}^{train} and X_{ij}^{test} are inde-

pendent. Unfortunately, choosing the appropriate p_i'' requires knowledge of the parameter p_i .

As p_i is typically unknown in practice, the authors suggest a simplification of the three-step process above in which X_{ij}^{both} is taken to be 0. Under this simplification, MCV becomes identical to count splitting (Step 0 of Algorithm 1 in the main text).

The authors’ explanation for setting $X_{ij}^{\text{both}} = 0$ is as follows. They imagine that X_{ij} counts the total number of unique molecules seen through two separate, shallower sequencing experiments (which gave rise to X_{ij}^{train} and X_{ij}^{test}). In this framework, X_{ij}^{both} denotes the molecules that were counted by both experiments and thus need to be subtracted out. The authors note that, since scRNA-seq experiments tend to be quite shallow (i.e. the values of p_i are small), the overlap between two even shallower experiments is likely to be negligible. We provide an alternate justification: when the p_i are small and the Ω_{ij} are large, then the Poisson approximation to the binomial distribution holds, and so independence is given by Proposition 1.

Thus, while developed for a different goal and under different assumptions, the procedure of Batson *and others* (2019) provides some justification for count splitting under a binomial assumption.

B. SIMULATION COMPARING COUNT SPLITTING TO SELECTIVE INFERENCE

Gao *and others* (2020) provide a selective inference approach for testing the null hypothesis that two clusters estimated via hierarchical clustering have the same mean vector, under an assumption of multivariate normality. More specifically, they assume

$$\mathbf{X} \sim \mathcal{MN}_{n \times q}(\mu, \mathbf{I}_n, \sigma^2 \mathbf{I}_q), \quad (\text{B.1})$$

and seek to test

$$H_0 : \bar{\mu}_{\hat{\mathcal{C}}_1} = \bar{\mu}_{\hat{\mathcal{C}}_2}, \quad (\text{B.2})$$

where $\hat{\mathcal{C}}_1$ and $\hat{\mathcal{C}}_2$ index the observations assigned to the two clusters and where, for any $G \subseteq$

$\{1, \dots, n\}$, we define $\bar{\mu}_G = \frac{1}{|i \in G|} \sum_{i \in G} \mu_i$. A naive Wald test for this null hypothesis does not control the Type 1 error rate because it ignores the fact that $\hat{\mathcal{C}}_1$ and $\hat{\mathcal{C}}_2$ are functions of the data X . Gao *and others* (2020) propose a selective Z-test that conditions on, among other things, the event that $\hat{\mathcal{C}}_1$ and $\hat{\mathcal{C}}_2$ were output by the hierarchical clustering algorithm. As shown in their paper, this method controls the Type 1 error rate when the data truly come from a multivariate normal distribution.

While not the focus of this paper, count splitting can also test the null hypothesis in (B.2) using a modification of Algorithm 1 from the main text.

To compare count splitting to selective inference in terms of Type 1 error rate control in this setting, we generate 1000 datasets where $n = 200, p = 10$ and $X_{ij} \sim \text{Poisson}(5)$. For each dataset, we do the following:

Naive: Run hierarchical clustering with average linkage on $\log(X+1)$ to obtain two clusters $\hat{\mathcal{C}}_1$ and $\hat{\mathcal{C}}_2$. Use the naive test described in Gao *and others* (2020) on $\log(X+1)$ to test $H_0 : \bar{\mu}_{\hat{\mathcal{C}}_1} = \bar{\mu}_{\hat{\mathcal{C}}_2}$. For this Wald test, estimate σ using the “conservative estimate” from Gao *and others* (2020).

Selective: Run hierarchical clustering with average linkage on $\log(X+1)$ to obtain two clusters $\hat{\mathcal{C}}_1$ and $\hat{\mathcal{C}}_2$. Use the selective test of Gao *and others* (2020) to test $H_0 : \bar{\mu}_{\hat{\mathcal{C}}_1} = \bar{\mu}_{\hat{\mathcal{C}}_2}$. Estimate σ using the “conservative estimate” from Gao *and others* (2020).

Count Split: Run Step 0 (count splitting) of Algorithm 1 with $\epsilon = 0.5$ to obtain X^{train} and X^{test} . Run hierarchical clustering with average linkage on $\log(X^{\text{train}}+1)$ to assign each cell to $\hat{\mathcal{C}}_1$ or $\hat{\mathcal{C}}_2$. Use the Wald test described in Gao *and others* (2020) on $\log(X^{\text{test}}+1)$ to test $H_0 : \bar{\mu}_{\hat{\mathcal{C}}_1} = \bar{\mu}_{\hat{\mathcal{C}}_2}$. For this Wald test, estimate σ using the “conservative estimate” from Gao *and others* (2020), computed on the test set.

The results of this experiment are shown in Figure 7. While selective inference improves upon the

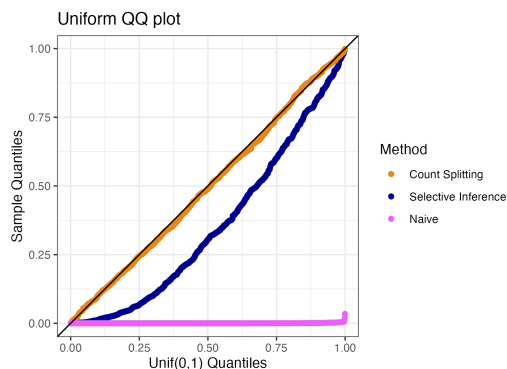


Fig. 7. Uniform QQ-plot of p-values under a global null. Count splitting controls the Type 1 error while selective inference does not.

naive method, Figure 7 shows that it fails to control the Type 1 error rate for log-transformed Poisson data. This illustrates why the dependence of selective inference on a normality assumption makes it inadequate for scRNA-seq applications.

C. IMPLEMENTATION DETAILS FOR FIGURE 1

In Figure 1, the naive method, cell splitting, and count splitting are all carried out as specified in Sections 3 and 4. The p-values reported are the default p-values returned by the `glm` function in **R** (Wald p-values).

The `jackstraw` **R** package (Chung *and others*, 2021) does not allow for fitting GLMs or for arbitrary latent variable estimation techniques. To obtain the jackstraw results for Figure 1, we implement the algorithm described in Section 3.6, which is similar to the proposal of Chung and Storey (2015) but allows for a GLM and an arbitrary latent variable estimation technique. We set $b = 100$ and $s = 10$ for our implementation.

The `pseudotimeDE` **R** package (Song *and others*, 2021) does allow for an arbitrary pseudotime estimation technique, but it fits negative binomial generalized additive models (GAMs) by default, and conducts likelihood ratio tests rather than Wald tests. To remain true to Song and Li (2021), the p-values for pseudotimeDE that are shown in Figure 1 are the default p-values returned by

their R package (i.e. from GAMs and not GLMs). We estimate pseudotime using the first principal component of the log transformed matrix (as for the other methods). We then pass this estimate of pseudotime into the R package's `runPseudotimeDE()` function with its default settings. To compute each empirical p-value, we use $B = 100$ subsets of the data, each containing 80% of the observations.

D. PROOF OF PROPOSITIONS FROM SECTION 4

D.1 *Proof of Proposition 2*

Note that $\mathbf{X}_{ij}^{\text{train}} \mid \{\mathbf{X}_{ij} = X_{ij}\} \sim \text{Binomial}(X_{ij}, \epsilon)$ and $\mathbf{X}_{ij}^{\text{test}} \mid \{\mathbf{X}_{ij} = X_{ij}\} \sim \text{Binomial}(X_{ij}, 1 - \epsilon)$. The first statement is by construction and the second follows from swapping the roles of successes and failures in the binomial experiment. We now derive the marginal variance of each distribution from the known conditional mean and variance:

$$\begin{aligned}
 \text{Var}(\mathbf{X}_{ij}^{\text{test}}) &= \text{E} [\text{Var} [\mathbf{X}_{ij}^{\text{test}} \mid \mathbf{X}_{ij}]] + \text{Var} [\text{E} [\mathbf{X}_{ij}^{\text{test}} \mid \mathbf{X}_{ij}]] \\
 &= \text{E} [(1 - \epsilon)\epsilon\mathbf{X}_{ij}] + \text{Var} [(1 - \epsilon)\mathbf{X}_{ij}] \\
 &= (1 - \epsilon)\epsilon\Lambda_{ij} + (1 - \epsilon)^2 \left(\frac{\Lambda_{ij}^2}{b_j} + \Lambda_{ij} \right) \\
 &= (1 - \epsilon)\Lambda_{ij} + \frac{(1 - \epsilon)^2\Lambda_{ij}^2}{b_j}, \\
 \text{Var}(\mathbf{X}_{ij}^{\text{train}}) &= \text{E} [\text{Var} [\mathbf{X}_{ij}^{\text{train}} \mid \mathbf{X}_{ij}]] + \text{Var} [\text{E} [\mathbf{X}_{ij}^{\text{train}} \mid \mathbf{X}_{ij}]] \\
 &= (1 - \epsilon)\epsilon\Lambda_{ij} + \epsilon^2 \left(\frac{\Lambda_{ij}^2}{b_j} + \Lambda_{ij} \right) \\
 &= \epsilon\Lambda_{ij} + \frac{\epsilon^2\Lambda_{ij}^2}{b_j}.
 \end{aligned}$$

Next note that

$$\text{Var}(\mathbf{X}_{ij}^{\text{train}}) + \text{Var}(\mathbf{X}_{ij}^{\text{test}}) = \Lambda_{ij} + \frac{(\epsilon^2 + (1 - \epsilon)^2)\Lambda_{ij}^2}{b_j},$$

and that since $\mathbf{X}_{ij} = \mathbf{X}_{ij}^{\text{train}} + \mathbf{X}_{ij}^{\text{test}}$,

$$\begin{aligned} \text{Cov}(\mathbf{X}_{ij}^{\text{train}}, \mathbf{X}_{ij}^{\text{test}}) &= \frac{1}{2} (\text{Var}(\mathbf{X}_{ij}) - \text{Var}(\mathbf{X}_{ij}^{\text{train}}) - \text{Var}(\mathbf{X}_{ij}^{\text{test}})) \\ &= \frac{1}{2} \left(\Lambda_{ij} + \frac{\Lambda_{ij}^2}{b_j} - \Lambda_{ij} - \frac{(\epsilon^2 + (1-\epsilon)^2)\Lambda_{ij}^2}{b_j} \right) \\ &= \frac{1}{2} \left(\frac{2(\epsilon(1-\epsilon))\Lambda_{ij}^2}{b_j} \right) = \frac{\epsilon(1-\epsilon)\Lambda_{ij}^2}{b_j}. \end{aligned}$$

Finally, to compute correlation, we divide by the covariance by

$$\begin{aligned} \sqrt{\text{Var}(\mathbf{X}_{ij}^{\text{train}}) \text{Var}(\mathbf{X}_{ij}^{\text{test}})} &= \sqrt{\left((1-\epsilon)\Lambda_{ij} + \frac{(1-\epsilon)^2\Lambda_{ij}^2}{b_j} \right) \left(\epsilon\Lambda_{ij} + \frac{\epsilon^2\Lambda_{ij}^2}{b_j} \right)} \\ &= \sqrt{(1-\epsilon)\epsilon\Lambda_{ij}^2 + \frac{[\epsilon(1-\epsilon)]\Lambda_{ij}^3}{b_j} + \frac{\epsilon^2(1-\epsilon)^2\Lambda_{ij}^4}{b_j^2}} \\ &= \frac{\Lambda_{ij}}{b_j} \epsilon(1-\epsilon) \sqrt{\frac{b_j^2}{\epsilon(1-\epsilon)} + \frac{b_j\Lambda_{ij}}{\epsilon(1-\epsilon)} + \Lambda_{ij}^2}. \end{aligned}$$

Putting it all together,

$$\begin{aligned} \text{Cor}(\mathbf{X}_{ij}^{\text{train}}, \mathbf{X}_{ij}^{\text{test}}) &= \frac{\frac{\epsilon(1-\epsilon)\Lambda_{ij}^2}{b_j}}{\frac{\Lambda_{ij}}{b_j} \epsilon(1-\epsilon) \sqrt{\frac{b_j^2}{\epsilon(1-\epsilon)} + \frac{b_j\Lambda_{ij}}{\epsilon(1-\epsilon)} + \Lambda_{ij}^2}} \\ &= \frac{\Lambda_{ij}}{\sqrt{\frac{b_j^2}{\epsilon(1-\epsilon)} + \frac{b_j\Lambda_{ij}}{\epsilon(1-\epsilon)} + \Lambda_{ij}^2}} \\ &= \frac{\sqrt{\epsilon(1-\epsilon)}}{\sqrt{\frac{b_j^2}{\Lambda_{ij}^2} + \frac{b_j}{\Lambda_{ij}} + \epsilon(1-\epsilon)}}, \end{aligned}$$

as claimed in Proposition 2.

D.2 Proof of Proposition 3

Let $X_{ij} \sim \text{Poisson}(\gamma_i \Lambda_{ij})$. First note that

$$\begin{aligned}
\text{Cov}(\mathbf{X}_{ij}, \mathbf{X}_{ij}^{\text{train}}) &= \mathbb{E} [\mathbf{X}_{ij} E [X_{ij}^{\text{train}} | X_{ij}]] - \mathbb{E}[\mathbf{X}_{ij}] E[\mathbf{X}_{ij}^{\text{train}}] \\
&= \epsilon \mathbb{E}[\mathbf{X}_{ij}^2] - \epsilon \gamma_i^2 \Lambda_{ij}^2 \\
&= \epsilon (\text{Var}(\mathbf{X}_{ij}) + \mathbb{E}[\mathbf{X}_{ij}]^2) - \epsilon \gamma_i^2 \Lambda_{ij}^2 \\
&= \epsilon (\gamma_i \Lambda_{ij} + \gamma_i^2 \Lambda_{ij}^2) - \epsilon \gamma_i^2 \Lambda_{ij}^2 \\
&= \epsilon \gamma_i \Lambda_{ij}.
\end{aligned}$$

Next, note that $\text{SD}(\mathbf{X}_{ij}) = \sqrt{\gamma_i \Lambda_{ij}}$ and $\text{SD}(\mathbf{X}_{ij}^{\text{train}}) = \sqrt{\epsilon \gamma_i \Lambda_{ij}}$. Thus, as claimed in Proposition 3,

$$\text{Cor}(\mathbf{X}_{ij}, \mathbf{X}_{ij}^{\text{train}}) = \frac{\epsilon \gamma_i \Lambda_{ij}}{\gamma_i \Lambda_{ij} \sqrt{\epsilon}} = \sqrt{\epsilon}.$$

D.3 Proof of Proposition 4

Let $\mathbf{X}_{ij} \sim \text{Poisson}(\gamma_i \exp(\beta_{0j} + \beta_{1j} L_i))$. The Fisher information matrix for the distribution of \mathbf{X}_j with respect to $\beta_j = (\beta_{0j}, \beta_{1j})$ is given by

$$\mathcal{I}(\beta_j) = [1_n \ L]^T \text{diag}(E[\mathbf{X}_j]) [1_n \ L]. \quad (\text{D.1})$$

We define $\tilde{\beta}_0 = \log(1 - \epsilon) + \beta_0$ and $\tilde{\beta}_1 = \beta_1$ such that, by Proposition 1, we can write the distribution of $\mathbf{X}_{ij}^{\text{test}}$ as $\text{Poisson}(\gamma_i \exp(\tilde{\beta}_{0j} + \tilde{\beta}_{1j} L_i))$. The Fisher Information matrix for the distribution of $\mathbf{X}_j^{\text{test}}$ with respect to $\tilde{\beta}_j = (\tilde{\beta}_0, \tilde{\beta}_1)$ is given by

$$\mathcal{I}(\tilde{\beta}_j) = [1_n \ L]^T \text{diag}(E[\mathbf{X}_j^{\text{test}}]) [1_n \ L] = (1 - \epsilon) [1_n \ L]^T \text{diag}(E[\mathbf{X}_j]) [1_n \ L] = (1 - \epsilon) \mathcal{I}(\beta_j). \quad (\text{D.2})$$

If we regress $\mathbf{X}_j^{\text{test}}$ on L , a Wald test for $H_0 : \tilde{\beta}_1 = 0$ is based on the approximate large sample null distribution:

$$\hat{\beta}_1(L, \mathbf{X}_j^{\text{test}}) \sim N\left(0, \left[I(\tilde{\beta}_j)^{-1}\right]_{22}\right).$$

If we regress \mathbf{X}_j on L , a Wald test for $H_0 : \beta_1 = 0$ is based on the approximate large sample null distribution:

$$\hat{\beta}_1(L, \mathbf{X}_j) \sim N\left(0, \left[\mathcal{I}(\beta_j)^{-1}\right]_{22}\right).$$

Thus, using (D.2), as claimed in Proposition 4,

$$\text{Var}\left(\hat{\beta}_1(L, \mathbf{X}_j^{\text{test}})\right) \approx \frac{1}{1-\epsilon} \text{Var}\left(\hat{\beta}_1(L, \mathbf{X}_j)\right).$$

E. OVERDISPERSION IN THE CARDIOMYOCYTE DATA

In Section 6, we fit Poisson GLMs to the cardiomyocyte differentiation data from Elorbany *and others* (2022). Here, we justify the use of Poisson GLMs (and the use of count splitting) by showing that the amount of estimated overdispersion is small.

We carry out the following process using the 10,000 cells from all 7 days of the differentiation protocol. We focus on the $p = 2,500$ high variance genes that we analyze in Section 6 of the main text (see Section F).

1. Compute $\hat{L}(X)$, using the function $\hat{L}(\cdot)$ used in Section 6 and elaborated on in Appendix F.
2. For $j = 1, \dots, p$, fit a negative binomial GLM using the `MASS` package in `R` to predict X_j using $\hat{L}(X)$. From each GLM, record the estimated overdispersion parameter \hat{b}_j , along with the predicted mean $\hat{\Lambda}_{ij}$ for $i = 1, \dots, n$ and $j = 1, \dots, p$.
3. Make a histogram of the $n \times p$ values of $\frac{\hat{\Lambda}_{ij}}{\hat{b}_j}$.

We note that the process above double dips in the data, and so the estimated values $\hat{\Lambda}_{ij}$ and \hat{b}_j may not be completely reliable. Here, we simply use them to understand the order of magnitude of the overdispersion.

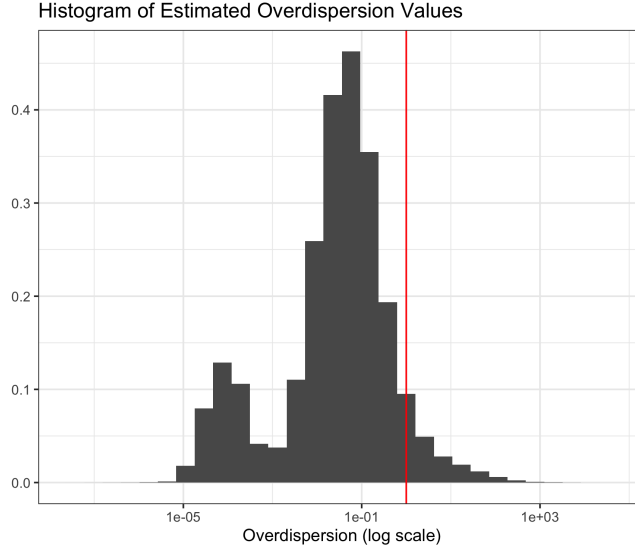


Fig. 8. Histogram of estimated values of $\frac{\Lambda_{ij}}{b_j}$ for the cardiomyocyte data. The vast majority of values are less than 1 (marked with a red vertical line).

The resulting histogram is shown in Figure 8. As noted in Section 4.2, the values of $\frac{\Lambda_{ij}}{b_j}$ indicate the amount of excess variance in the data. Figure 8 shows that, for the cardiomyocyte data, the vast majority of these values are less than 1. Thus, despite the presence of a few datapoints with very large values of overdispersion, we decided to fit Poisson GLMs (which are more numerically stable than negative binomial GLMs) for the analysis in Section 6. As shown in Figure 2 of the main text, count splitting performs reasonably well when $\frac{\Lambda_{ij}}{b_j} \leq 1$.

F. DETAILS OF PSEUDOTIME ESTIMATION FROM SECTION 6

Let M be the raw gene expression matrix. We now describe the procedure used to compute $\hat{L}(\cdot)$ in Section 6.

Steps 1–3 largely follow the pre-processing choices made in Elorbany *and others* (2022), whereas Steps 4–5 use the popular and user-friendly **Monocle3** R package for trajectory estimation and are motivated by the **Monocle3** vignettes (Pliner *and others*, 2020).

1. **Normalization:** We create the log-normalized matrix with the (i, j) th entry given by $\log\left(\frac{M_{ij}}{\hat{\gamma}_i(M)} + 1\right)$. All operations below are run on this log-normalized matrix. The $\hat{\gamma}(\cdot)$ function is the `librarySizeFactors()` function from the `scran` package (Lun *and others*, 2016), which computes the row sums of M and then scales them to have a geometric mean of 1.
2. **Estimate Cell Cycle:** Using the `tricycle` package (Zheng *and others*, 2022), estimate the cell cycle phase for each cell using the log-normalized version of M .
3. **Feature selection:** We apply the `modelGeneVar()` function from the `scran` package. This function computes the mean and the variance of each log-normalized gene, and then fits a trend to these values. The residuals from this trend measure the biological component of variation for each gene. We then run the `getTopHVGs()` from the `scran` package, which ranks the genes by this estimated biological component and computes a p-value to test the null hypothesis that this biological component is equal to 0. We select the genes whose biological component is significantly greater than 0 with a false discovery rate cutoff of 0.005. If more than 2500 genes are deemed significant, we retain the top 2500 of these selected genes for further analysis. While this feature selection is performed separately for the training dataset, test dataset, and full dataset inside of the $\hat{L}(\cdot)$ function, the 2500 genes whose p-values are plotted in Figure 6 of the main text are the top 2500 genes selected using the full dataset (rather than the training dataset or the test dataset).
4. **Preprocessing and alignment and regressing out:** We reduce the dimension of the matrix output by the previous step (log-normalized with at most 2,500 features) by keeping only the top 100 principal components of this matrix. Using the reduced dimension matrix, we then regress out technical sources of variation using the method of Haghverdi *and others* (2018), as implemented in the `Monocle3` package in the function `align.cds()`. We include cell line as the alignment group, and we additionally regress out the estimated cell cycle

phase (from Step 2) and the proportion of mitochondrial reads. While this regression step is suggested in the `Monocle3` vignettes, regressing out the estimated cell cycle phase is perhaps less standard. Regressing out cell cycle is particularly important for the “day 0 only” example, as we want to ensure that no true trajectory (including a trajectory through the cell cycle) is present in the “day 0 only” data.

5. **Monocle3 dimension reduction, graph embedding, and pseudotime calculation:**

Next, we compute pseudotime using a sequence of functions from the `Monocle3` package. All functions are run with their default settings unless otherwise noted. The input to this step is the matrix output by the previous step. First, we run `reduce_dimension()`, which takes the already dimension-reduced data and turns it into a two-dimensional UMAP representation. Next, we run `cluster_cells()`. (While we do not wish to estimate clusters, this is a required step of the `Monocle3` pipeline.) We next run `learn_graph()`, but we let `use_partition=FALSE` so that `Monocle3` ignores cluster information and learns a single graph through all of the cells. The clustering and graph steps both happen in UMAP space. Finally, we run `order_cells()`, which projects all cells onto the principal graph to obtain a single continuous trajectory. As `order_cells()` requires a user-specified “root” cell (the cell which will have a pseudotime of 0), we choose the induced pluripotent stem cell (IPSC) that is closest to a vertex of the graph as the “root” cell. The cell type labels (i.e. the labels that allow us to identify IPSC cells) were computed by Elorbany *and others* (2022).